Teng Shiwen (Orcid ID: 0000-0003-3436-7882)
Liu Chao (Orcid ID: 0000-0001-7049-493X)
Zhang Zhibo (Orcid ID: 0000-0001-9491-1654)
Wang Yuan (Orcid ID: 0000-0001-6657-8401)
Sohn Byung-Ju (Orcid ID: 0000-0001-6134-3515)

Retrieval of Ice-Over-Water Cloud Microphysical and Optical Properties Using Passive Radiometers

Shiwen Teng[1,2], Chao Liu[1,2,*], Zhibo Zhang[3], Yuan Wang[4], Byung-Ju Sohn[2,5], and Yuk L. Yung[4]

[1]Collaborative Innovation Center on Forecast and Evaluation of Meteorological Disasters, Nanjing University of Information Science & Technology, Nanjing, China.

[2]Key Laboratory for Aerosol-Cloud-Precipitation of China Meteorological Administration, School of Atmospheric Physics, Nanjing University of Information Science & Technology, Nanjing, China.

[3]Department of Physics, University of Maryland, Baltimore County (UMBC), Baltimore, MD, USA.

[4]Division of Geological and Planetary Science, California Institute of Technology, Pasadena, CA, USA.

[5]School of Earth and Environmental Sciences, Seoul National University, Seoul, South Korea.

Corresponding author: Chao Liu (chao_liu@nuist.edu.cn)

Key Points:

- A cloud microphysical and optical property retrieval algorithm for ice-over-water clouds using passive satellite observations is developed

- The absorptivity differences of water and ice at three shortwave-infrared channels are used to differentiate between water and ice clouds

- The retrieved cloud optical properties are found to be significantly improved, compared to MODIS-derived properties

Abstract

Current satellite cloud products from passive radiometers provide effective single-layer cloud properties by assuming a homogeneous cloud in a pixel, resulting in inevitable biases when multiple-layer clouds are present in a vertical column. We devise a novel method to retrieve cloud vertical properties for ice-over-water clouds using passive radiometers. Based on the absorptivity differences of liquid and ice clouds at four shortwave-infrared channels (centered at 0.87-, 1.61-, 2.13-, and 2.25-µm), cloud optical thicknesses (COT) and effective radii of both upper-layer ice and lower-layer liquid water clouds are inferred simultaneously. The algorithm works most effectively for clouds with ice COT<7 and liquid water COT>5. The simulated spectral reflectances based on our retrieved ice-over-water clouds become more consistent with observations than those with a single-layer assumption. This new algorithm will improve our understanding of clouds, and we suggest that these four cloud channels should be all included in future satellite sensors.

Plain Language Summary

Over a quarter of clouds in the atmosphere overlap in a vertical column, and ignoring the cloud vertical distribution may significantly influence estimation of their radiative effects. However, information about cloud vertical structures is mostly provided by in situ or active instruments with limited spatiotemporal resolution. Cloud properties from satellite passive radiometer observations are derived by treating a cloud pixel as a single-layer cloud, resulting in biases in our understanding of clouds and their radiative forcing. This study improves the capabilities of passive radiometers for retrieving properties of ice-over-water clouds, including the optical thickness and effective radii of both upper ice and lower liquid water clouds simultaneously. Our method provides a new perspective for radiometers-based retrieval of multilayer cloud properties, and will improve the evaluation of cloud radiative effects.

1 Introduction

Clouds have an important role in the atmospheric circulation and energy budget, and its multilayered feature is one of the major uncertainties in cloud observations, weather and climate modeling (Wang and Rossow, 1998; Boucher et al., 2013). Multilayer clouds are frequently studied using surface, aircraft and satellite observations (Tian and Curry, 1989; Dong and Mace, 2003). The occurrence of multilayer clouds is as large as 25% globally (Chang and Li, 2005; Yuan and Oreopoulos, 2013; Wang et al., 2016), and becomes even larger over the Southern Ocean and higher latitudes of both hemispheres (Wind et al., 2010).

Accurate characterization of multilayer clouds is crucial not only for Earth's and atmospheric radiative budget but also for weather and climate modeling. Cloud radiative forcing (CRF) is highly dependent on their location and optical and microphysical properties (Liang and Wang, 1997; Chen et al., 2000; Wang et al., 2020). Based on cloud properties from both active and passive satellite sensors over one year, Kato et al. (2011) reported that the simplification of multilayer clouds based on the Moderate-resolution Imaging Spectroradiometer (MODIS) single-layer cloud properties may overestimate global annual mean irradiances by 12.5W/m^2 for shortwave and 2.5W/m^2 for longwave at the top of atmosphere (TOA). Meanwhile, Li et al. (2011) estimated that the zonal mean shortwave CRF differences between multi- and single-layer clouds at the TOA could reach 120W/m^2 in the tropics. Simple parameterizations of multilayer clouds in the general circulation models (GCMs) also introduce large biases in cloud cover and CRF (Takahashi et al., 2017). Neggers et al. (2011) indicated that accounting for the small-scale overlap for cumuliform cloud in GCM can change the TOA shortwave CRF by -20 to -40W/m^2.

Due to the importance of multilayer clouds on the global radiation budget, much work has been devoted to better characterize those clouds (González et al., 2002; Watts et al., 2011; Poulsen et al., 2012). Hu et al. (2007) derived the optical depths of thin cirrus above opaque liquid water clouds using active Cloud-Aerosol Lidar and Infrared Pathfinder Satellite Observation (CALIPSO). Combing microwave and visible-infrared measurements, Huang et al. (2006) developed an advanced multilayer cloud retrieval system, and the retrieved ice water path is more consistent with the radar-derived one. In current cloud retrieval efforts for satellite passive radiometers, the assumption is made that a single cloud layer exists in a given pixel due to processing constraints. Thus, multilayer clouds are retrieved as single-layer ice clouds in the MODIS cloud products, and this can result in large errors in the ice cloud optical and microphysical properties (Marchant et al., 2020). Only some multilayer cloud identification products are introduced, e.g., for MODIS (Platnick et al., 2017), the Polarization and Directionality of the Earth's Reflectance (POLDER) (Bréon, 2016) and the Visible Infrared Imaging Radiometer Suite (VIIRS) (Wang et al., 2019). Sourdeval et al. (2015; 2016) made a progress to simultaneously retrieve the optical and microphysical properties of multilayer clouds using radiometric measurements at five channels ranging from visible to thermal infrared wavelength. Besides, few quantitative multilayer cloud optical or microphyscial property product from only radiometers has been introduced yet.
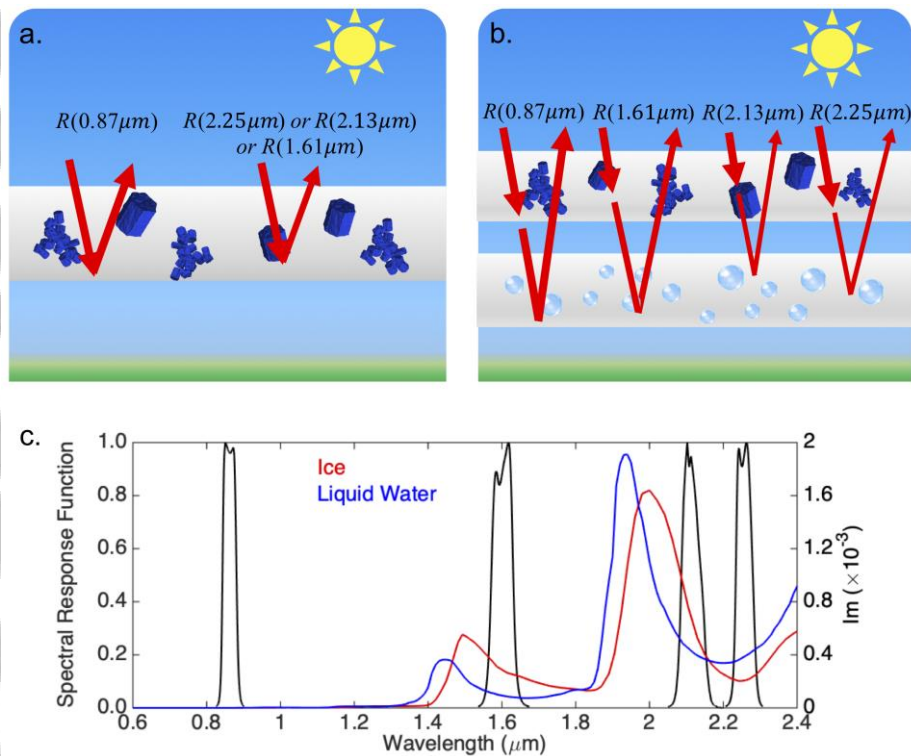
Cloud absorptivity differences in different phases at shortwave-infrared (SWIR) channels show potential for inferring multilayer cloud properties, and were recently used for multilayer cloud detection (Miller et al., 2014; Wang et al., 2018; 2019). Miller et al. (2014) probed ice/mixed below liquid-topped clouds using observations at the 1.61- and 2.25-µm channels. The combination of the 2.13- and 2.25-µm channels provides more information on cloud phase detection than either channel alone (Coddington et al., 2017). Wang et al. (2019) developed a VIIRS multilayer cloud detection algorithm relying on the 1.6-2.25-µm channel pair. These cloud absorbing channels are qualitatively utilized to detect cloud phase or multilayer clouds, whereas have not been quantitatively used to explore multilayer cloud properties.

This study introduces an algorithm to retrieve multilayer cloud properties by exploiting the different SWIR absorptivities of ice and liquid water clouds. This study focuses on the ice-over-water clouds, i.e., an upper-layer ice cloud overlapping a lower-layer liquid water cloud in the same atmospheric column, which are the most common multilayer clouds with occurrences over 50% (Wang et al., 2000; Sourdeval et al., 2016).

2 Sensitivities of shortwave-infrared channels

The schematics of the conventional Nakajima-King algorithm (Nakajima and King, 1990) and our retrieval algorithm are shown in Figures 1a and 1b, respectively. In the conventional retrieval, a cloud pixel is simply assumed to have an equivalent, homogeneous single-layer cloud, i.e., either ice or liquid water; this becomes problematic if both ice and liquid water clouds exist in the same pixel. To mitigate this limitation, we attempt to retrieve the cloud properties of both ice and liquid water clouds using radiometer observations. Thus, ice-over-water clouds in a pixel are assumed to include one ice and one water layer, each of which is homogeneous. In contrast to the Nakajima-King algorithm that infers two unknowns, a total of four unknowns, including ice cloud optical thickness (COT) and effective radius (CER), and liquid water COT and CER, are contained to characterize ice-over-water clouds. The cloud height assumption will not significantly affect the retrieval, because only solar channels are considered and atmospheric gas absorption and scattering are negligible compared to cloud impacts. Also, the potential underestimation of COT resulting from partly cloudy in a

pixel is not considered. To obtain the unknowns, at least four independent observations should be assembled for each retrieval.


Figure 1. The effects of absorptivity differences of SWIR channels on radiative transfer for (a) common single-layer clouds and (b) ice-over-water clouds. (c) The imaginary part of the complex refractive index for ice (red) and liquid water (blue) as a function of wavelength, and spectral response functions of four SWIR channels (centered at 0.87-, 1.61-, 2.13-, and 2.25-μm) are given by black lines.

Figure 1c illustrates the imaginary part of the refractive index of ice and liquid water, and the spectral response functions of three VIIRS channels (centered at 0.87-, 1.61- and 2.25-μm, respectively) and one MODIS channel (centered at 2.13-μm). The imaginary part reveals the absorptivity differences of ice and liquid water clouds. The imaginary part of 0.87-μm channel is close to 0, indicating no absorption, and those of the three absorbing SWIR channels show obvious differences. Absorptivity of ice particles is the strongest at the 2.13-μm channel, followed by the 1.61- and 2.25-μm channels. The liquid water absorptivities at the 2.13- and 2.25-μm channels are similar, and both are stronger than that at the 1.61-μm channel. The ice absorptivities at the 1.61- and 2.13-μm channels are stronger than that of liquid water cloud, while the absorptivity of ice clouds at the 2.25-μm channel is weaker than that of liquid water cloud. Such features make the reflectances of ice-over-water clouds at SWIR channels different.

We further examine the specific sensitivity of the aforementioned four channels to ice-over-water cloud properties. Reflectances are simulated using a rigorous 128-stream Discrete-Ordinate-Method Radiative Transfer (DISORT, Thomas and Stamnes, 1999) model, and both ice and water cloud optical properties are the same as those used for the NASA MODIS Collection 6.1 (C6.1) product (Platnick et al., 2017). Each channel shows a unique sensitivity to ice-over-water cloud properties. In particular, the 0.87-μm channel has the largest sensitivity

to COT, the 1.61-µm channel displays the largest sensitivity to ice CER, while the 2.25-µm channel is most sensitive to liquid water CER (Details see Text S1 and Figure S1).

To better understand the degree of information available in these channels, we apply an information content (IC) analysis (Shannon, 1948; Wang et al., 2016). The degree of freedom (DOF) is used to quantify the number of independent pieces of information given by satellite measurements (Rodgers, 2000). The DOF calculation is detailed in Text S2. The DOF value ranges from 0 to the number of parameters to be retrieved, and larger values of DOF indicate more information available for a retrieval.
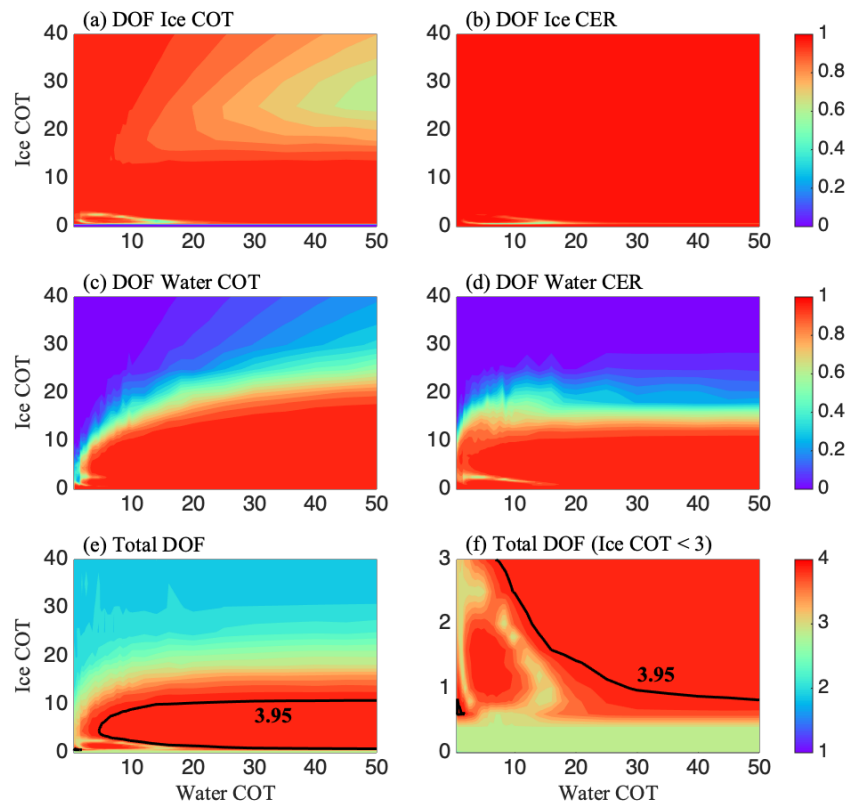
Figure 2. (a-d) Partial DOF for ice COT, ice CER, liquid water COT, and liquid water CER, respectively; (e) total DOF theoretically calculated for an ice-over-water cloud case with ice CER = $30\mu m$ and liquid water CER = $12\mu m$; and (f) Similar to panel (e) but only for ice-over-water clouds with thin upper ice clouds. The black solid lines correspond to total DOF of 3.95.

Figure 2 shows partial and total DOFs at different ice and liquid water COTs (ice COT ranging from 0.01 to 40 and liquid water COT ranging from 0.5 to 50). Typical values for ice and liquid water CER (30µm and 12µm) are considered, and simulations with other CER combinations show similar results (not shown). Figures 2a - 2d are the partial DOFs with respect to the four cloud parameters. Almost all the partial DOFs are larger than 0.8, even up to 1.0, when ice COT < 15. When the upper-layer ice cloud is thick (COT > 15) or the liquid water COT is relatively small, the lower-layer liquid water cloud becomes invisible, and partial DOFs decrease rapidly, especially for liquid water COT and CER. The DOF of ice COT is small when ice COT < 0.5, because SWIR channels are naturally limited on detecting optically thin clouds. Similarly, the total DOF in Figure 2e is 4 at the maximum, indicating that in

principle four parameters can be retrieved. Total DOF with ice COT < 3 is shown in Figure 2f. The black solid lines highlight the 3.95 contour line of the total DOF, mostly over the region with ice COT < 7 and liquid water COT > ~5. The region showing total DOF ≥ 3.95 would have enough information for the retrieval of the four parameters. However, if ice COT < 0.5 or > 15, the total DOF drastically decreases to 3.0, or even 2.0. In other words, it is difficult to infer the optical and microphysical properties of ice-over-water clouds when ice COT is either relatively small (< 0.5) or large (> 15).

Besides the sensitivity of measurements to retrieved cloud parameters, information content of measurements also depends on the uncertainties associated with observations, forward model and *a priori* assumption (Rodgers, 2000). Figure S2 illustrates the expected total retrieval uncertainties on the four parameters resulting from a combination of all these uncertainties. Both uncertainties of ice and liquid water COT are less than 20% when ice COT is smaller than 7 and liquid water COT is larger than 5, whereas uncertainties of ice and liquid water CER are larger and can be as high as 40%. For regions where DOF is not saturated, the uncertainties would be much larger.

3 Retrieval of ice-over-water cloud properties

We now perform our retrieval on actual satellite observations. The orbits of VIIRS onboard Suomi-NPP and MODIS onboard Aqua become close to each other every two to three days. Thus, it becomes possible to collect Level-1b reflectances at the aforementioned four channels (three VIIRS ones and one MODIS) over the same region for ice-over-water cloud property retrievals. To be more specific, we collocate the VIIRS Level-1b reflectances to MODIS grids through the weighted averaging approach (Lai et al., 2019), and the observational time difference between VIIRS and MODIS is constrained to be within 5 mins. Additionally, both the VIIRS multilayer cloud mask (following Wang et al., 2019) and the MODIS C6.1 multilayer cloud flags are collocated for identifying multilayer cloud pixels. A pixel that is classified as multilayer clouds by VIIRS or that has MODIS multilayer cloud flag value larger than 5 is regarded as an ice-over-water cloud pixel, and our retrieval is performed to infer COTs and CERs of both upper ice and lower liquid water clouds within the pixel. An optimal estimation method is used for the retrieval (Rodgers, 2000; Xu et al., 2018), and detailed descriptions of the retrieval procedure are described in Text S3 and Table S1.

Figure 3 shows an example over the South Atlantic Ocean. A region between 40°S ~ 46°S and 20°W ~ 35°W is considered with collocated MODIS and VIIRS data available, and details of satellite observations are found in Table S2. The top panels of Figure 3 show the MODIS-derived cloud phase, COT, and CER from the MODIS C6.1 Level-2 cloud product (MYD06), which are based on the single-layer homogeneous cloud assumption (i.e., Figure 1a). In the middle and right panels, the red and blue colors indicate properties of ice and liquid water clouds, respectively. Figure 3d presents the multilayer cloud flag from MODIS C6.1 cloud product, and as the value increases, the confidence level of multilayer clouds increases. Most clouds between 25°W and 30°W are detected to have an ice-over-water structure, and other regions appear to be mostly covered by liquid water clouds. It is evident, in a comparison of Figure 3a with 3d, that a large amount of ice-over-water clouds have to be simplified as single-layer ice clouds by MODIS product, and some pixels with unreasonably large ice COT and small ice CER pixels are noticed in the MODIS product.
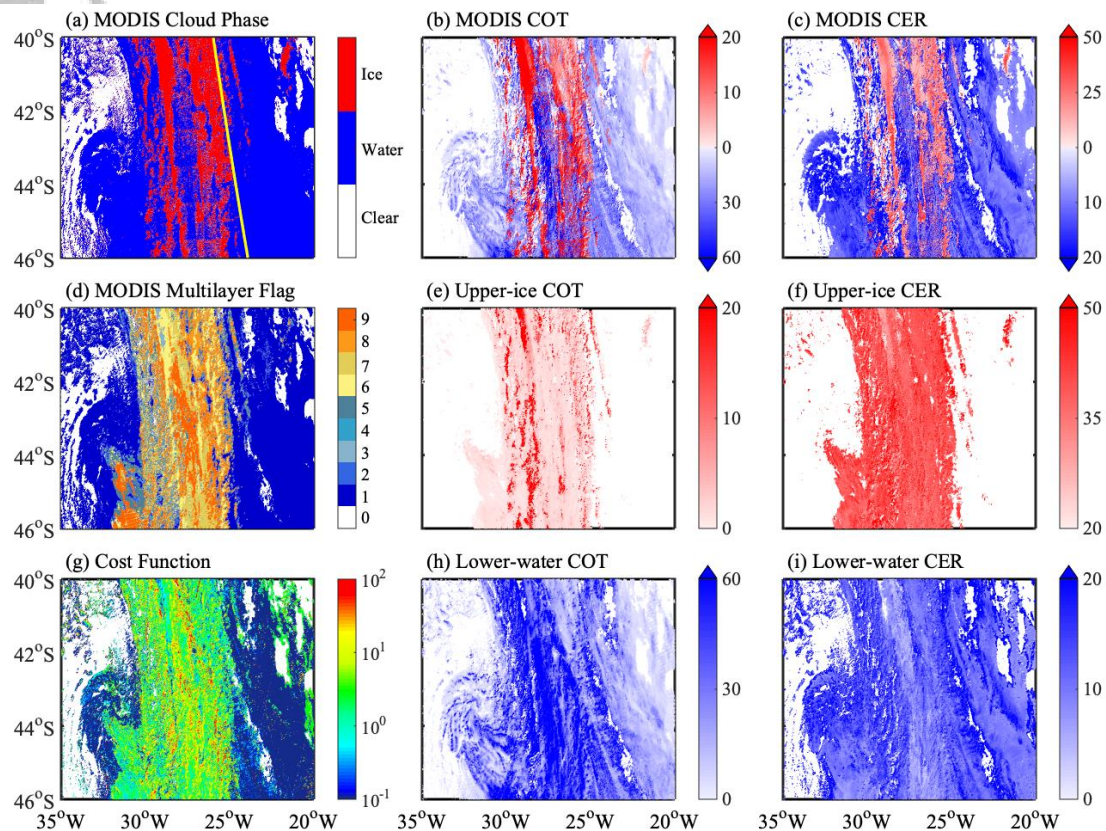
Figure 3. (a) MODIS/Aqua cloud phase for case study taken on 18 December 2017 at 15:50 UTC over the South Atlantic Ocean; (b) MODIS-derived COT; (c) MODIS-derived CER; (d) MODIS cloud multilayer flag: 0 indicates clear-sky, 1 indicates single layer cloud, 2-9 indicates increasing confidence level of the presence of multilayer cloud; (e) retrieved upper-ice COT; (f) retrieved upper-ice CER; (g) Retrieved cost function; (h) retrieved lower-water COT; and (i) retrieved lower-water CER.

The retrieved ice-over-water cloud properties are given in Figure 3e (ice COT), 3f (ice CER), 3h (liquid water COT), and 3i (liquid water CER). The upper-layer ice clouds tend to be optically thin and homogeneous with COTs mostly smaller than 8 (Figure 3e) and CER values of between 30 and 50 µm (Figure 3f), and the lower-layer liquid water clouds have COTs larger than 10 (Figure 3h) and CER values ranging from a few to 30 µm (Figure 3i). Detailed frequency distributions of the four retrieved parameters are shown in Figure S3. Clearly, when ice-over-water clouds are present, the total COT would be underestimated if the retrieval were to treat the pixel as an ice cloud, and overestimated if the retrieval were to treat the pixel as a liquid water cloud. For total COTs, the single-layered MODIS COTs are generally smaller than those of ice-over-water clouds. MODIS COTs are mostly ranging from 10 to 30, while ice-over-water-based retrievals give more than 70% of pixels with COT larger than 20 (See from Figure S4). However, the differences may be affected by many factors, e.g., cloud top height, cloud phase used for single-layer cloud-based retrieval, and so on. As a result, either positive or negative COT biases can be introduced. Additionally, significant differences can be found for single- and two-layer CER from Figures 3c, 3f and 3i.

Finally, Figure 3g presents the cost function for our retrievals, and cost function values are lower than the dimension of measurement vector (i.e. 4 in this study) for successful retrievals. The cost functions of single-layer clouds are smaller than 0.1 (successfully retrieval

ratio > 95%), indicating the stability of the conventional method for single-layer clouds. The results for ice-over-water clouds are less robust, and only over 75% of pixels result in cost functions smaller than 4 (see from the frequency histogram in Figure S5). Clearly, this result indicates that most of our retrievals can be trusted, at least to achieve agreement between observations and forward simulations. The uncertainties of our retrieved results can be estimated through IC analysis as discussed in Section 2.
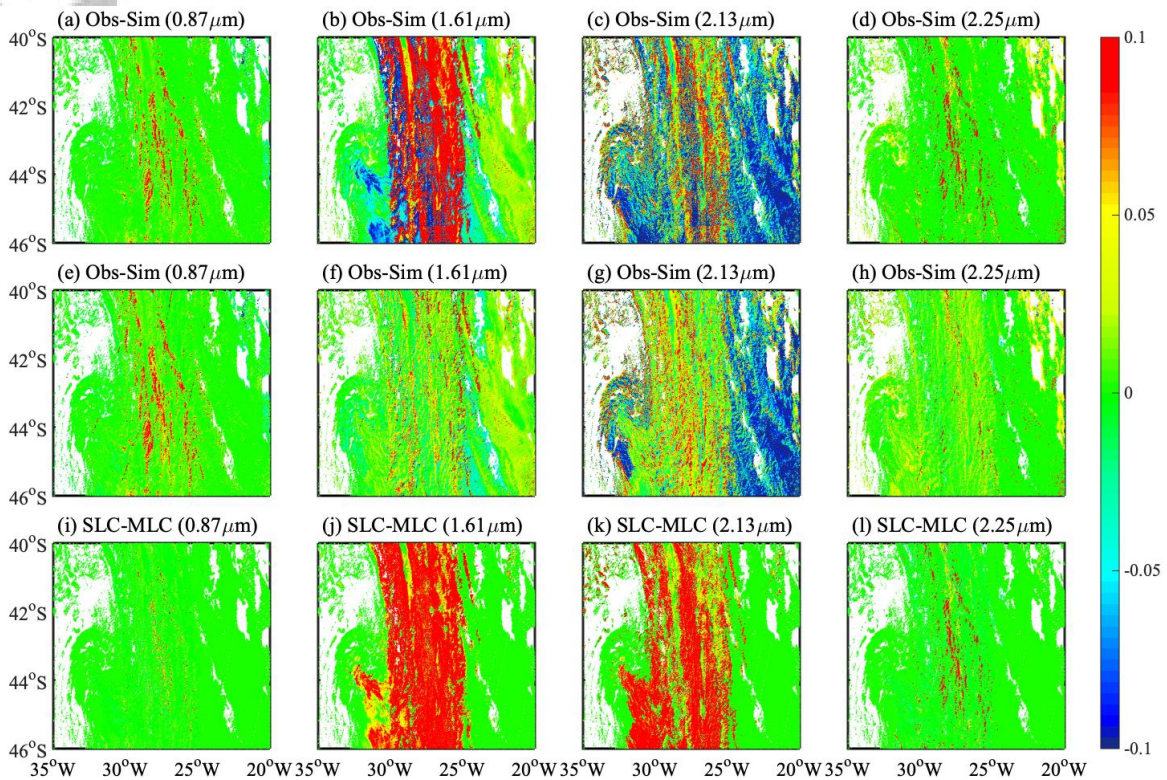

Figure 4. Reflectance differences at 0.87-, 1.61-, 2.13-, and 2.25-μm channels. (Top panels) Reflectance differences between measurements and simulations based on single-layer cloud model; (Middle panels) Reflectance differences between measurements and simulations based on the ice-over-water cloud model; (Bottom panels) Reflectance differences between single-layer cloud and multilayer cloud models (SLC - MLC).

The reflectance differences between observed and simulated reflectance at 0.87-, 1.61-, 2.13-, and 2.25-μm channels are analyzed in Figure 4. First, forward radiative transfer simulations are performed based on a single-layer cloud configuration (Figure 1a structure) and corresponding single-layer retrieved properties (the 0.87- and 2.25-μm channel retrievals), and the top panels illustrate the differences between satellite observations and these simulated results (i.e. Obs - Sim). The middle panels are similar, but the simulations are based on ice-over-water clouds and our retrieved cloud properties in Figures 3e, 3f, 3h and 3i. The bottom panels are differences between the top and middle panels. Simulations based on single-layer cloud properties can well represent the observed reflectance at VIIRS 0.87- and 2.25-μm channels, whereas biases at 1.61- and 2.13-μm channels are quite significant, especially for the region with ice-over-water clouds. Meanwhile, owing to different viewing angles for MODIS and VIIRS and 3-D radiative effects of clouds, the reflectance difference at MODIS 2.13-μm channel for single-layer liquid water cloud regions is also relatively large. By contrast, reflectance differences for all channels are substantially reduced using the ice-over-water cloud retrieval algorithm (middle panels), especially for the 1.61- and 2.13-μm channels, with

reflectance differences mostly within 0.05. It is clear from the bottom panels that the reflectance differences between simulations and obervations at 1.61- and 2.13-μm channels are reduced by more than 0.1 after considering ice-over-water clouds information. In other words, by introducing the potential presence of ice-over-water cloud properties, the interpretation of the spectral reflectances can be greatly improved compared to those based on single-layer clouds. In summary, our method for inferring ice-over-water cloud properties offers a reasonable approach for improving the interpretation of these complex scenes.
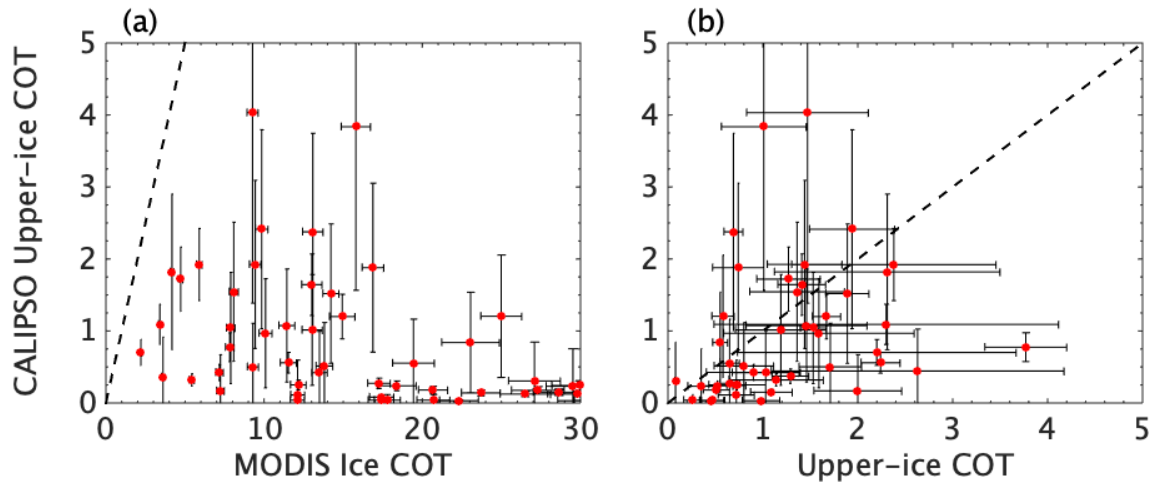
Figure 5. Comparison between CALIPSO-derived upper-ice COT and (a) MODIS-derived ice COT; (b) retrieved upper-ice COT in ice-over-water clouds. The black dashed lines are 1:1 lines. The black solid lines represent respective retrieval uncertainties (absolute errors).

To further illustrate the advantage of our ice-over-water cloud property retrieval, we perform another evaluation. The CALIPSO data are considered as the "truth" of cloud vertical distribution, and the corresponding track is shown by the yellow line in Figure 3a. Because CALIPSO retrieval works most reliably for relatively thin clouds (Holz et al., 2016), we consider the retrieved ice COTs here. The MODIS operational ice COT and the upper-layer ice COT based on our algorithm are compared to the CALIPSO-derived upper-layer ice COT in Figures 5a and 5b, respectively. Error bars represent their corresponding retrieval uncertainties. Compared to CALIPSO-estimated COTs, the MODIS single-layer product results in an unacceptable overestimation of ice COTs, even after taking the uncertainties into account. Meanwhile, our algorithm results in ice COT retrievals that are much closer to those from CALIPSO, even if some differences are still present. The uncertainties shown from our algorithm seem relatively larger than those from MODIS products, because solar channels are essentially less sensitive to optically thin ice clouds. Overall, our algorithm significantly improves the consistency of retrieved ice COTs.

4 Conclusion

This study develops a novel algorithm to characterize ice-over-water cloud properties using only solar channels available on the MODIS and VIIRS sensors. The retrieval algorithm takes the advantages of the absorptivity differences of liquid water and ice clouds at four SWIR channels, and is applied to collocated MODIS and VIIRS measurements to infer ice and liquid water cloud optical and microphysical properties simultaneously. The combined four channels provide sufficient information for inferring ice-over-water cloud optical thickness and effective particle size. Both numerical evaluation and our results indicate the algorithm is particularly

effective for the case of ice-over-water cloud with ice COT smaller than 7 and an optically thicker liquid water cloud (water COT > 5). With actual retrievals in our case study, over 75% ice-over-water pixels can be well constrained, and retrievals clearly improve the multispectral reflectance consistency between measurements and forward simulations. With upper ice and lower water COTs separated, our retrieved ice COTs agree with CALIPSO results more closely than those of MODIS product.

Our results indicate that global satellite remote sensing of ice-over-water cloud properties is feasible, and the resulting retrieval product can better constrain the cloud radiative forcing and Earth's energy budget, which will be the topic of a future study. Our method also provides a potential opportunity for the retrieval of other mixed/multilayer clouds (water-over-ice and mixed-phased clouds), because the channel reflecntance differences can be essentially influenced by cloud phases and microphysical properties, not siginficaitnly by their vertical locations. Further, our method could help to improve an infrared-based cloud property retrieval (Iwabuchi et al., 2014), owing to the less sensitivity of infrared channels to thick clouds with COT larger than 5.

Last but not least, most current satellite radiometers only include two of the three required cloud absorbing channels, i.e. 1.61-μm and 2.13/2.25-μm. Our study suggests that serious consideration be given for inclusion of the 1.61-, 2.13-, and 2.25-μm channels in future satellite radiometer designs for accurate cloud characterizations.

Acknowledgments, Samples, and Data

References

Boucher, O., Randall, D., Artaxo, P., Bretherton, C., Feingold, G., Forster, P., & et al. (2013), Clouds and aerosols. In Climate change 2013: The physical science basis. Contribution of Working Group I to the Fifth Assessment Report of the Intergovernmental Panel on Climate Change (pp. 571-657). Cambridge University Press. doi:10.1017/CBO9781107415324.016

Bréon, F.-M. (2016), POLDER/Parasol leval-2 product data format and user manual. CEA/LSCE, CNES, France

Chang, F. L., & Li, Z. (2005), A near-global climatology of single-layer and overlapped clouds and their optical properties retrieved from Terra/MODIS data using a new algorithm. *J. Clim.*, *18*, 4752-4771. doi:10.1175/JCLI3553.1

Chen, T., Rossow, W. B., & Zhang, Y. (2000), Radiative effects of cloud-type variations. *J. Clim.*, *13*(1), 264-286. doi:10.1175/1520-0442(2000)013<0264:REOCTV>2.0.CO;2

Coddington, O. M., Vukicevic, T., Schmidt, K. S., & Platnick, S. (2017), Characterizing the information content of cloud thermodynamic phase retrievals from the notional PACE OCI shortwave reflectance measurements. *J. Geophys. Res. Atmos.*, *122*, 8079-8100. doi:10.1002/2017JD026493

Dong, X., & Mace, G. G. (2003), Profiles of low-level stratus cloud microphysics deduced from ground-based measurements. *Journal of Atmospheric and Oceanic Technology*, *20*, 42-53. doi:10.1175/1520-0426(2003)020<0042:POLLSC>2.0.CO;2

González, A., Wendling, P., Mayer, B., Gayet, J.-F., & Rother, T. (2002), Remote sensing of cirrus cloud properties in the presence of lower clouds: An ATSR-2 case study during the Interhemispheric Differences in Cirrus Properties From Anthropogenic Emissions (INCA) experiment. *J. Geophys. Res. Atmos.*, *107*(D23), 4693. doi:10.1029/2002JD002535

Holz, R. E., Platnick, S., Meyer, K., Vaughan, M., Heidinger, A., Yang, P., & et al. (2016), Resolving ice cloud optical thickness biases between CALIOP and MODIS using infrared retrievals. *Atmos. Chem. Phys.*, *16*, 5075-5090. doi:10.5194/acp-16-5075-2016

Hu, Y., Vaughan, M., Liu, Z., Powell, K., & Rodier, S. (2007), Retrieving optical depths and lidar ratios for transparent layers above opaque water clouds from CALIPSO lidar measurements. *IEEE Geoscience and Remote Sensing Letters*, *4*(4), 523-526. doi:10.1109/LGRS.2007.901085

Huang, J., Minnis, P., Lin, B., Yi, Y., Fan, T.-F., Sun-Mack, S., & Ayers, J. K. (2006), Determination of ice water path in ice-over-water cloud systems using combined MODIS and AMSR-E measurements. *Geophys. Res. Lett.*, *33*, L21801. doi:10.1029/2006GL027038

Iwabuchi, H., Yamada, S., Katagiri, S., Yang, P., & Okamoto, H. (2014), Radiative and microphysical properties of cirrus cloud inferred from infrared measurements made by the Moderate Resolution Imaging Spectroradiometer (MODIS). Part I: Retrieval method. *Journal of Applied Meteorology and Climatology*, *53*(5), 1297-1316. doi:10.1175/JAMC-D-13-0215.1

Kato, S., Rose, F. G., Sun-Mack, S., Miller, W. F., Chen, Y., & et al. (2011), Improvements of top-of-atmosphere and surface irradiance computations with CALIPSO-, CloudSat-, and MODIS-derived cloud and aerosol properties. *J. Geophys. Res.*, *116*, D19209. doi:10.1029/2011JD016050

Lai, R., Teng, S., Yi, B., Letu, H., Min, M., Tang, S., & Liu, C. (2019), Comparison of cloud properties from Himawari-8 and Fengyun-4A geostationary satellite radiometers with MODIS cloud retrievals. *Remote Sens.*, *11*(14), 1703. doi:10.3390/rs11141703

Li, J., Yi, Y., Minnis, P., Huang, J., Yan, H., Ma, Y., Wang, W., & Ayers, J. K. (2011), Radiative effect differences between multi-layered and single-layer clouds derived from CERES, CALIPSO, and CloudSat data. *J. Quant. Spectrosc. Radiat. Transfer*, *112*, 361-375. doi:10.1016/j.jqsrt.2010.10.006

Liang, X. Z., & Wang, W. C. (1997), Cloud overlap effects on GCM climate simulations. *J Geophys. Res.*, *102*(D), 11039-11047. doi:10.1029/97JD00630

Marchant, B., Platnick, S., Meyer, K., and Wind, G. (2020), Evaluation of the Aqua MODIS collection 6.1 multilayer cloud detection algorithm through comparisons with CloudSat CPR and CALIPSO CALIOP products. *Atmos. Meas. Tech.*, *13*, 3263-3275. doi:10.5194/amt-13-3263-2020

Miller, S. D., Noh, Y.-J., & Heidinger, A. K. (2014), Liquid-top mixed-phase cloud detection from shortwave-infrared satellite radiometer observations: A physical basis. *J. Geophys. Res. Atmos.*, *119*, 8245-8267. doi:10.1002/2013JD021262

Nakajima, T., Tanaka, M., & King, M. D. (1990), Determination of the optical thickness and effective particle radius of clouds from reflected solar radiation measurements, Part I: Theory. *J. Atmos. Sci.*, *47*, 187-193. doi:10.1175/1520-0469(1990)047<1878:DOTOTA>2.0.CO;2

Neggers, R. A. J., Heus, T., & Siebesma, A. P. (2011), Overlap statistics of cumuliform boundary-layer cloud fields in large-eddy simulations. *J. Geophys. Res.*, *116*, D21202. doi:10.1029/2011JD015650

Platnick, S., Meyer, K. G., King, M. D., & et al. (2017), The MODIS cloud optical and microphysical products: Collection 6 updates and examples from Terra and Aqua. *IEEE T. Geosci. Remote Sensing*, *55*(1), 502-525. doi:10.1109/TGRS.2016.2610522

Poulsen, C. A., Siddans, R., Thomas, G. E., Sayer, A. M., Grainger, R. G., Campmany, E., Dean, S. M., Arnold, C., & Watts, P. D. (2012), Cloud retrievals from satellite data using optimal estimation: evaluation and application to ATSR. *Atmos. Meas. Tech.*, *5*(8), 1889-1910. doi:10.5194/amt-5-1889-2012

Rodgers, C. D. (2000), Inverse Methods for Atmospheric Sounding: Theory and Practice. World Scientific Pub Co Inc.

Shannon, C. E. (1948), A mathematical theory of communications. *Bell Syst. Tech. J.*, *27*, 379-423. doi:10.1002/j.1538-7305.1948.tb01338.x

Sourdeval, O., C-Labonnote, L., Baran, A. J., & Brogniez, G. (2015), A methodology for simultaneous retrieval of ice and liquid water cloud properties. Part I: Information content and case-study. *Q. J. R. Meteorol. Soc.*, *141*, 870-882. doi:10.1002/qj.2405

Sourdeval, O., C-Labonnote, L., Baran, A. J., Mülmenstädt, J., & Brogniez, G. (2016), A methodology for simultaneous retrieval of ice and liquid water cloud properties. Part 2: Near-global retrievals and evaluation against A-Train products. *Q. J. R. Meteorol. Soc.*, *142*, 3063-3081. doi:10.1002/qj.2889

Takahashi, H., Lebsock, M., Suzuki, K., Stephens, G., & Wang, M. (2017), An investigation of microphysics and subgrid-scale variability in warm-rain clouds using the A-Train observations and a multiscale modeling framework. *J. Geophys. Res. Atmos.*, *122*, 7493-7504. doi:10.1002/2016JD026404

Thomas, G. E., & Stamnes, K. (1999), Radiative Transfer in the Atmosphere and Ocean. Cambridge Univ. Press, New York.

Tian, L., & Curry, J. A. (1989), Cloud overlap statistics. *J. Geophys. Res. Atmos.*, *94*, 9925-9935. doi:10.1029/JD094iD07p09925

Wang, C., Platnick, S., Zhang, Z., Meyer, K., & Yang, P. (2016), Retrieval of ice cloud properties using an optimal estimation algorithm and MODIS infrared observations: 1. Forward model, error analysis, and information content. *J. Geophys. Res. Atmos.*, *121*, 5809-5826. doi:10.1002/ 2015JD024526

Wang, J., & Rossow, W. B. (1998), Effects of cloud vertical structure on atmospheric circulation in the GISS GCM. *J. Clim.*, *11*, 3010-3029. doi:10.1175/1520-0442(1998)011<3010:eocvso>2.0.co;2

Wang, J., Rossow, W. B., & Zhang, Y. (2000), Cloud vertical structure and its variations from a 20-year global rawinsonde dataset. *J. Clim.*, *13*, 3041-3056. doi:10.1175/1520-0442(2000)013<3041:CVSAIV>2.0.CO;2

Wang, T., Fetzer, E. J., Wong, S., Kahn, B. H., & Yue, Q. (2016), Validation of MODIS cloud mask and multilayer flag using CloudSat-CALIPSO cloud profiles and a cross-reference of

their cloud classifications. *J. Geophys. Res. Atmos.*, *121*, 11620-11635. doi:10.1002/2016HD025239

Wang, J., Liu, C., Min, M., Hu, X., Lu, Q., & Husi, L. (2018), Effects and applications of satellite radiometer 2.25-μm channel on cloud property retrievals. *IEEE T. Geosci. Remote Sensing*, *56*, 5207-5216. doi:10.1109/TGRS.2018.2812082

Wang, J., Liu, C., Yao, B., Min, M., Letu, H., Yin, Y., & Yung, Y. L. (2019), A multilayer cloud detection algorithm for the Visible Infrared Imager Radiometer Suite (VIIRS). *Remote Sens. Environ.*, *227*, 1-11. doi:10.1016/j.rse.2019.02.024

Wang, Y., Su, H., Jiang, J. H., Xu, F., & Yung, Y. (2020), Impact of cloud ice particle size uncertainty in a climate model and implications for future satellite missions. *J. Geophys. Res. Atmos.*, *125*, 6. doi:10.1029/2019JD032119

Watts, P. D., Bennartz, R., & Fell, F. (2011), Retrieval of two-layer cloud properties from multispectral observations using optimal estimation. *J. Geophys. Res.*, *116*, D16203. doi:10.1029/2011JD015883

Wind, G., Platnick, S., King, M. D., & et al. (2010), Multilayer cloud detection with the MODIS near-infrared water vapor absorption band. *J. Appl. Meteorol. Climatol.*, *49*, 2315-2333. doi:10.1175/2010JAMC2364.1

Xu, F., van Harten, G., Diner, D. J., Davis, A. B., Seidel, F. C., Rheingans, B., & et al. (2018), Coupled retrieval of liquid water cloud and above-cloud aerosol properties using the Airborne Multiangle SpectroPolarimetric Imager (AirMSPI). *J. Geophys. Res. Atmos.*, *123*, 3175-3204. doi:10.1002/2017JD027926

Yuan, T., & Oreopoulos, L. (2013), On the global character of overlap between low and high clouds. *Geophys. Res. Lett.*, *40*, 5320-5326. doi:10.1002/grl.50871